

## Maximization of Workspace Volume of 3-DOF Spatial Parallel Manipulators

Karol Miller

Department of Mechanical and Materials Engineering,  
The University of Western Australia, Crawley/  
Perth WA 6009, Australia  
e-mail: kmiller@mech.uwa.edu.au

*In this work we investigate the influence of motor axes orientation on the workspace volume of 3-DOF manipulators, showing that the Delta configuration is not optimal. The configuration characterized by  $\alpha = \text{ArcTan}(1/\sqrt{2}) \approx 35.26^\circ$ —the inclination of each motor axis to the horizontal plane (for the Delta robot  $\alpha = 0^\circ$ ), and  $\beta = 60^\circ$ —the rotation of each motor with respect to the vertical axis (for the Delta robot  $\beta = 0^\circ$ ), known as the New University of Western Australia Robot (NUWAR) is shown to be advantageous over the Delta configuration in terms of workspace volume and shape. These results led to the construction of a prototype and an Australian Patent application.*

[DOI: 10.1115/1.1462621]

**Keywords:** Parallel Robot, Workspace Maximization

### 1 Introduction

Parallel robots, unlike serial, traditional ones, have the end-effector connected to the base by several kinematic chains in parallel. Research into the field of parallel robots documented in the literature dates back to the year 1938, when Pollard patented his mechanism for car painting [1]. In 1947 Mc Gough proposed a six-degree-of-freedom platform, which was later used by Stewart in his flight simulator [2]. Parallel manipulators are particularly suited to a number of typical industrial applications and have been of interest to various researchers over the years. In recent years several new structures and mechanisms have been developed for a variety of both established and novel applications, such as packaging, assembly, haptic interfaces, etc. [3–8].

Parallel manipulators possess a number of advantages when compared to traditional serial arms. They offer generally a much higher rigidity and smaller mobile mass than their serial counterparts. These features allow much faster and more precise manipulations. A catalogue of a large variety of parallel configurations can be found in the book by Merlet [9] and at his internet page [10].

Contributed by the Mechanisms and Robotics Committee for publication in the JOURNAL OF MECHANICAL DESIGN. Manuscript received August 2000. Associate Editor: S. K. Agrawal.

The DELTA robot [3] is an original design that arose from the need detected in the production and manufacturing sectors for manipulators better suited to the fast execution of light-duty tasks. As seen from Fig. 1, the three closed kinematic chains consisting of arms and parallel rods, are identical and actuated by three revolute electric motors rigidly mounted on the top (robot base), and closed below at the common toolbase by ball joints. The combi-

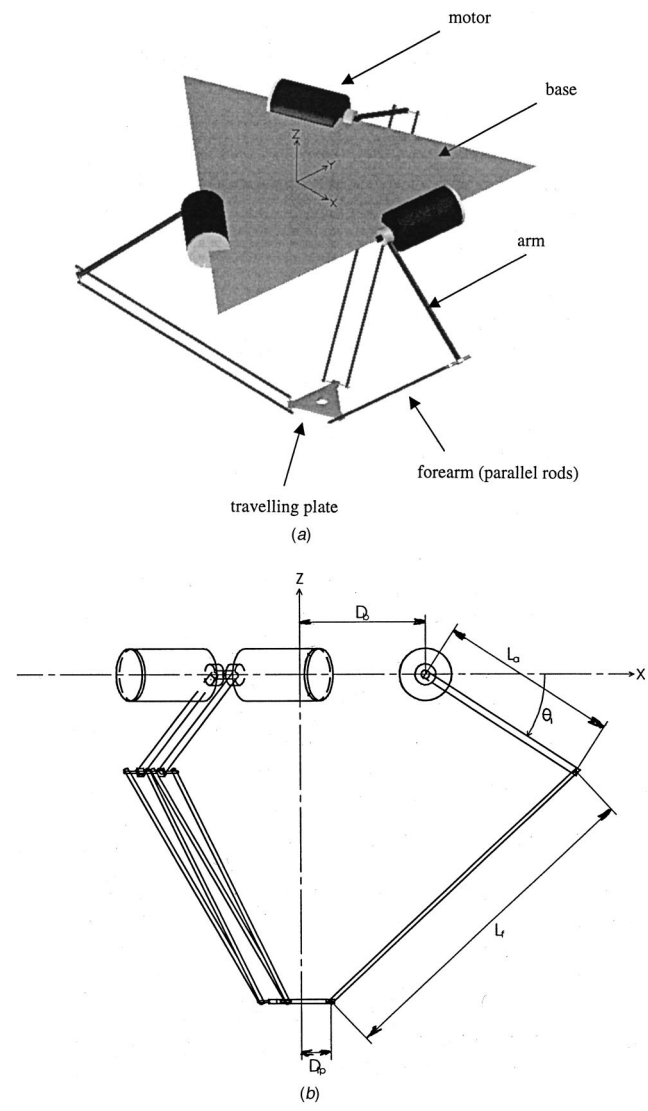


**Fig. 1 (a) Layout of the Delta robot; (b) dimensional parameters of the Delta robot**

**Table 1 Dimensions of the New UWA Robot.**

length of the arm from joint to joint	$L_a = 0.26 \text{ m}$
length of the forearm from joint to joint	$L_f = 0.48 \text{ m}$
radial distance of each motor from the centerline	$D_b = 0.194 \text{ m}$
displacement in radial direction of the midpoint of a revolute joint on the travelling plate, $D = D_b - D_{tp}$	$D_{tp} = 0.03 \text{ m}$
spacing of the forearms	$S_f = 0.05 \text{ m}$
angular limit of lateral rotation of the universal joints, which join the arms to the forearms	$\phi = 60^\circ$

nation of the constrained motion of these three chains results in three translatory degrees of freedom for the robot tool-base. The structure is very rigid. Its lowest natural frequency is approx. 120 Hz. Capable of achieving  $500 \text{ m/s}^2$ , the direct drive DELTA robot is one of the fastest robots in the world.

This paper considers the feasibility of various layouts for three-degree-of-freedom parallel robots, and discusses the potential advantages and disadvantages of different architectures. Like the Delta, the robots considered in this paper consist of three kine-

**Table 2 Volume of workspace, with respect to volume of workspace of the Delta robot,  $\alpha=0^\circ$  and  $\beta=0^\circ$ .**

		$\beta$									
		0	10	20	30	40	50	60	70	80	90
$\alpha$	0	1.0000	0.9654	0.9027	0.8196	0.7331	0.6535	0.5808	0.5258	0.4954	0.4846
	10	0.9304	0.9919	1.0031	0.9692	0.9127	0.8523	0.7823	0.7323	0.6985	0.6877
	20	0.8165	0.9150	0.9946	1.0381	1.0300	1.0004	0.9654	0.9273	0.8981	0.8831
	30	0.7238	0.8488	0.9435	1.0223	1.0712	1.0804	1.0608	1.0558	1.0442	1.0358
	<b>35.26</b>	<b>0.6992</b>	<b>0.8300</b>	<b>0.9265</b>	<b>1.0112</b>	<b>1.0581</b>	<b>1.0912</b>	<b>1.0938</b>	<b>1.1062</b>	<b>1.0873</b>	<b>1.0904</b>
	40	0.6900	0.8162	0.9200	0.9988	1.0546	1.0873	1.1058	1.1135	1.1154	1.1173
	50	0.7262	0.8185	0.9104	0.9812	1.0400	1.0765	1.0958	1.1096	1.1108	1.1173
	60	0.8004	0.8688	0.9358	0.9938	1.0492	1.0819	1.0969	1.1142	1.1050	1.1185
	70	0.9050	0.9504	0.9996	1.0373	1.0692	1.0800	1.1173	1.1200	1.1273	1.1365
	80	1.0035	1.0296	1.0512	1.0742	1.0896	1.1131	1.1231	1.1246	1.1300	1.1358
	90	1.0785	1.0785	1.0785	1.0792	1.0788	1.0785	1.0785	1.0785	1.0785	1.0785

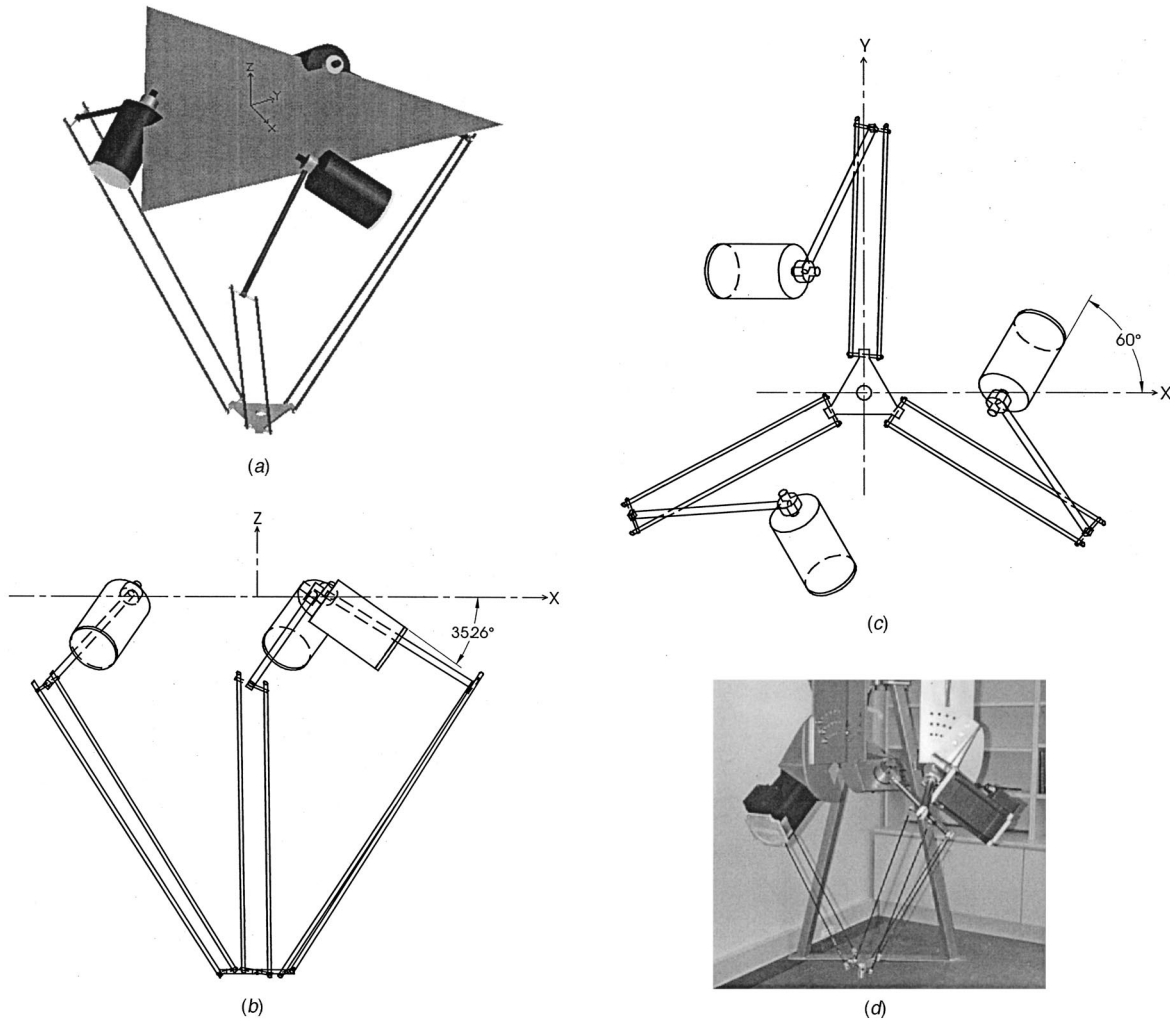


**Fig. 2** New University of Western Australia Robot—NUWAR with design variables: angles  $\alpha=35.26^\circ$  and  $\beta=60^\circ$ : (a) general view; (b) bottom view; (c) side view; (d) NUWAR prototype

matic chains in parallel, which connect the base to the end-effector. It is of particular interest to determine, for given dimensions of a manipulator, how the size and shape of the robot workspace varies with values of two angles defining the orientations of the motor axes. Finding the optimal values of these angles, from the point of view of the workspace volume, was an initial objective of this study. Based on the workspace volume and shape analysis, a new mechanism is proposed and a prototype constructed—the New University of Western Australia Robot.

## 2 The Workspace of Delta-Type Manipulators—Effect of Motor Axis Orientation

The robots analyzed in this study are variations of the Delta Robot, Fig. 1. The arm/forearm assemblies are identical, and located symmetrically on the sides of an equilateral triangle. In all models the Z axis is perpendicular to the base plane and points vertically up. The X and Y axes are located in the base plane, with the X axis pointing towards motor #1. The origin is located at the point equidistant to the three motors.

The computer models of the robots were written parametrically so that different configurations can easily be analyzed. The mechanical simulation package ADAMS [11] and AutoCad/AutoLisp [12] were used. In addition to the dimensions of each component, two design variables—angles  $\alpha$  and  $\beta$ —are introduced:  $\alpha$  measures the inclination of each motor to the horizontal; a positive value rotates the motor in a clockwise direction when viewed from the outside (for the Delta robot  $\alpha=0^\circ$ ), and  $\beta$ —rotation of each motor with respect to the vertical (Z) axis (for the Delta robot  $\beta=0^\circ$ ). These two angles determine the orientation of each motor axis (i.e. the controlled revolute joint axes), which connect the arms to the base. As the arm is rigidly attached to its motor axis, the angles  $\alpha$  and  $\beta$  control the orientation of the three arm/forearm assemblies. Varying  $\alpha$  and  $\beta$  angles leaves the locations of the three motors unchanged.

All dimensions have been chosen as in the DELTA-740 [13], see Table 1.

The robot's workspace was derived using AutoCAD. A generalized program was written using AutoLISP in terms of the design variables mentioned above. For each layout (i.e. different values of  $\alpha$  and  $\beta$ ), there exist equivalent configurations, which are mirror images, or  $180^\circ$  rotations of the original layout. Due to this "equivalence", it is only necessary to consider  $\alpha$  and  $\beta$  in the range from 0 to  $90^\circ$ .

It is also of interest to note that the motor axes are orthogonal to each other when  $\alpha=\text{ArcTan}(1/\sqrt{2})\approx 35.26^\circ$ . Also, when  $\beta=60^\circ$  motor axes become parallel to the opposite sides of the base triangle. The volumes of the workspace on one side of the base plane were calculated for  $\alpha$  and  $\beta$  between 0 to  $90^\circ$ , using  $1^\circ$  spacing between consecutive layouts. In total  $91\times 91=8281$  volume calculations were performed.

The results for a ten by ten grid of the design variables are shown in Table 2. The volume of the workspace varies widely as  $\alpha$  and  $\beta$  change. The layouts of interest are those, which have the workspace volume greater than that of the Delta robot. The maximum volume is about 13% larger than that of the Delta robot. There is a range of values of  $\alpha$  and  $\beta$  for which the workspace volume is close to this maximum value. These larger workspace volumes occur when  $\alpha$  is in the range of  $0.5\beta$  to  $0.8\beta$  (for all values of  $\beta$ ). The workspace is also large (1.08 times Delta) when  $\alpha=90^\circ$ . The shape of the workspace also varies widely as  $\alpha$  and  $\beta$  change.

It is evident that the Delta configuration is not optimal in terms of the workspace volume. Other feasible configurations occur in the range  $\alpha>30^\circ$  and  $\beta>50^\circ$  degrees.

Because the motor axes are orthogonal when  $\alpha=35.26^\circ$  degrees and they are parallel to the sides of the base triangle when  $\beta=60^\circ$ , this configuration—known as the New University of Western Australia Robot-NUWAR, Fig. 2—was chosen for a more

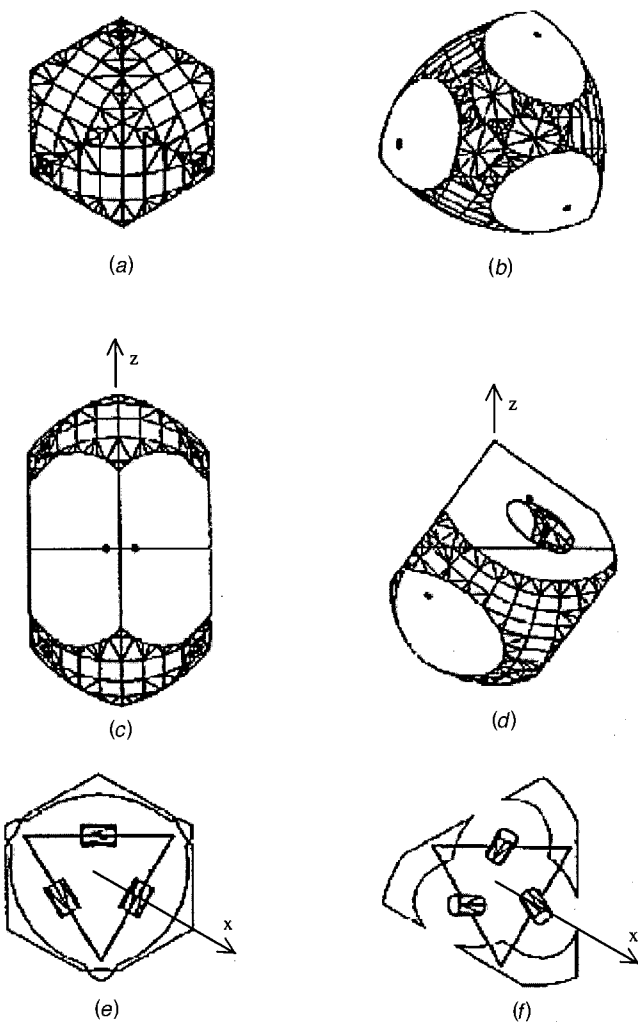


**Fig. 3 Workspace of the NUWAR and Delta robots (manipulator dimensions are listed in Table 1): (a) bottom view of the Delta robot's workspace; (b) bottom view of the NUWAR's workspace; (c) side view of the Delta robot's workspace. Note that the workspace is symmetric with respect to the base-plane, however only bottom half is usable; (d) side view of the NUWAR's workspace. Note that the workspace is not symmetric with respect to the base-plane; (e) base-plane section of the Delta's workspace, bottom view; (f) base-plane section of the NUWAR's workspace, bottom view.**

detailed analysis. The workspace of NUWAR is 9.4% larger than the workspace of the Delta, assuming all dimensions being the same.

Figure 3 presents workspaces of the NUWAR and Delta robots. Delta's workspace is symmetrical with respect to the base-plane, Fig. 3c. However, only (bottom) half of this workspace can be utilized in practice. NUWAR's workspace is not symmetrical (Fig. 3d) but the useful bottom half is larger than that of the Delta.

Close examination of the shape of the NUWAR's workspace (Fig. 3d) reveals that it has a larger cross section in the region closer to the base plane ( $z>-0.35$  m), but a smaller cross section further from the base-plane ( $z<-0.35$  m), in comparison to the workspace of the Delta, Fig. 3c. Hence, this robot would be more suitable for applications where a larger workspace is required close to the base-plane, which is typically the case in the light duty pick-and-place applications.

### 3 NUWAR Prototype

The results of numerical simulations formed a basis for a construction of a prototype [14]. The robot (Fig. 2d) is actuated by three high-torque BSM100B-2250 AC servomotors. The amplifiers chosen are DBSC 1110 AAAW AC Servo Drives. The control of the robot is executed by a PMAC-Lite four-axis controller. This equipment was supplied by Australian Baldor [15].

Additional refinement in the design of NUWAR's kinematic arrangement was the replacement of the ball joints connecting the parallelograms to the arms and the traveling plate, by pin joints [8,16]. This improvement allows for more robust mechanism, with higher torsional rigidity. Also, the manufacturing of the NUWAR mechanism employing pin joints is simpler.

The maximum acceleration achievable by NUWAR's travelling plate, as measured by motor angular encoders and transformed to the task space using the model of manipulator kinematics, is about  $600 \text{ m/s}^2$ .

### 4 Discussion and Conclusions

This paper presents the mechanics of the New University of Western Australia Robot—optimally structured Delta-type parallel robot. Maintaining all dimensions, and therefore, the size of the robot, unchanged, the influence of motor axes orientation (angles  $\alpha$  and  $\beta$ ) on robot's workspace volume and shape was researched. The results show that the configuration of the New University of Western Australia Robot—NUWAR is advantageous over the Delta configuration in terms of workspace volume. The shape of the workspace of NUWAR is beneficial for applications involving manipulations relatively close to the base plane.

### Acknowledgments

The author would like to thank most sincerely Mr. Matthew Jayarama for his help during the initial stages of the project, and numerous undergraduate students involved in building the prototype. This work was funded by the Faculty of Mathematical and Engineering Sciences of The University of Western Australia Research Launching Grant and the Australian Research Council.

### References

- [1] Pollard, W. L., 1938, "Position Controlling Apparatus," US Patent No. 2,286,571, June 16, 1942.
- [2] Stewart, D., 1966, "A Platform With Six Degrees of Freedom," *Proc. Inst. Mech. Eng.*, **180**, part I, (15), pp. 371–386.
- [3] Clavel, R., 1988, "Delta, a Fast Robot With Parallel Geometry," *Proc. of 18th International Symposium on Industrial Robots*, Lausanne, Switzerland, pp. 91–100.
- [4] Badano, F., Betemps, M., Burckhardt, C. W., Clavel, R., and Jutard, A., 1993, "Assembly of Chamferless Parts using a Fast Robot," *Proc. of 24th International Symposium on Industrial Robots*, Tokyo, pp. 89–96.
- [5] Herve, J. M., 1994, "Methodological Design of New Parallel Robots via the Lie Group of Displacements," *Proc. of CISM/IFTOMM Conference Ro.Man.Sy. '94*, Gdansk, pp. 301–306.
- [6] Pierrot, F., Dauchez, P., and Fournier, A., 1991, "Hexa, a fast 6-Degree of Freedom Fully Parallel Robot," *Proc. of International Conference on Advanced Robotics*, Pisa, **2/2**, pp. 1158–1163.
- [7] Arai, T., and Tanikawa, T., 1996, "Development of a New Parallel Manipulator With Fixed Linear Actuator," *Proc. of Japan/USA Symposium on Flexible Automation*, **1**, pp. 145–149.
- [8] Tsunaki, Y., Narusew, H., Nenchev, D. N., and Uchiyama, M., "Design of Compact 6-dof Interface," *Proc. of 1998 IEEE Conference on Robotics and Automation*, pp. 2581–2585.
- [9] Merlet, J. P., 1990, *Les robots parallèles*, Hermès, Paris.
- [10] Merlet, J. P., [http://www-sop.inria.fr/saga/pesonne/merlet/merlet\\_eng.html](http://www-sop.inria.fr/saga/pesonne/merlet/merlet_eng.html)
- [11] ADAMS Reference Manual, 1993 Version 7.0, Mechanical Dynamics, Ann Arbor, Michigan.
- [12] AutoCad Release 14 Users Guide, 1997 Autodesk, Inc.
- [13] Guglielmetti, P. (1994) "Model-Based Control of Fast Parallel Robots: a Global Approach in operational Space," PhD thesis no. 1228, Swiss Federal Institute of Technology, Lausanne.
- [14] Miller, K., 1998, "Parallel Robot," Australian Provisional Patent Application, No. PP7518.
- [15] Baldor Motors and Drives, 1997, *Australian Stock Product Catalogue, Australian Baldor Pty Limited*.
- [16] Tsai, L. W., 1997, "Multi-Degree-of-Freedom Mechanisms for Machine Tools and the Like," U.S. Patent No. 5,656,905.

## Optimized Kinematic Properties for Stevenson-Type Presses With Variable Input Speed Approach

Hong-Sen Yan<sup>1</sup>

Professor, Department of Mechanical Engineering,  
National Cheng Kung University, Tainan 70101, Taiwan,  
ROC

Wei-Ren Chen

Associate Professor, Department of Mechanical Engineering,  
Kun Shan University of Technology, Yung Kang City, Tainan Shien, 71048, Taiwan, ROC

*Traditionally, the input speed of a Stevenson-type press is constant. Here, we propose a novel approach by varying the input speed of the crank to make the ram's motion suitable for both deep-drawing and precision-cutting. This approach uses a servomotor as the power input. By properly designing the input speed, the output motion can pass through a desired trajectory. The input motion characteristics are planned with Bezier curves. Optimization is used to improve the output characteristics. Guidelines for defining the optimization problems are discussed. Additional dimensional synthesis is also suggested for reducing the input speed variation. Design examples are given for illustration.*

[DOI: 10.1115/1.1456163]

### 1 Introduction

Stevenson-type mechanisms are widely used in presses because of their structural simplicity for drawing process, but seldom for cutting. The presses are driven by electric motors that run at constant speed. The desired output motions are achieved by dimensional synthesis of the links. This paper presents an alternative approach by varying the crank's speed of the press to obtain various desired output motions. With a properly controlled servomotor, a press can be programmed to perform various processes, e.g., cutting, forming, and drawing.

Ulas and Craggs [1] verified that the mechanical state of a material can be represented as a point on the stress-strain-strain rate surface. Dies were designed with very special and complicated shapes to maintain the state of material along the optimal curve. However, if we can vary the input speed of the press, the required optimal drawing process can be obtained through the use of simple die shapes.

In the past years, Tesar and Matthew [2] derived the motion equations of the follower by considering the variable speed cams. Yan et al. [3–6] contributed to improve the motion characteristics of the follower acceleration by servo solutions. Connor et al. [7] discussed path generation problems of a 5-bar linkage with one input link driven by a variable-speed servomotor. Herman et al.

<sup>1</sup>To whom all correspondence should be addressed

Contributed by the Mechanism and Robotics Committee for publication in the ASME JOURNAL OF MECHANICAL DESIGN. Manuscript received Apr. 1999. Associate Editor: C. Innocenti.

[8] used hybrid cam mechanisms to reduce the peak power of the servomotor. And, Yossifon et al. [9] produced a servomotor-driven multi-action press. They further [10–12] used the characteristics of a servomotor to generate a press that provides constant force during working.

The purpose of this study is to design, for Stevenson-mechanisms, a general input speed trajectory and useful geometric properties that lead to desired ram motion for cutting and forming processes.

## 2 The System

Figure 1 shows the flow chart of the proposed system. The goal is to design a feasible variable input speed trajectory that satisfies the desired output motion characteristics of the ram. Bezier curves and optimization methods are applied for providing a satisfactory speed trajectory. And, kinematic analysis is performed for achieving the desired output motion characteristics. However, if the input/output results are not satisfactory, the dimensional properties of the press can also be considered as the design variables. The PID method, not discussed in this paper, can be used to control the servomotor for driving the input link along the derived speed trajectory.

## 3 Bezier Curve

Since the input link of the press is a crank undergoing a circular rotation, we define the displacement trajectory of the crank by an  $n$ th order Bezier curve  $\theta(t)$ , as shown in Fig. 2, with parameter  $t$  as:

$$\theta(t) = \sum_{i=0}^n \theta_i B_{i,n}(t) + \theta_{UDC} \quad (1)$$

where

$$B_{i,n}(t) = \frac{n!}{i!(n-i)!} \cdot t^i \cdot (1-t)^{n-i} \quad t \in [0,1] \quad (2)$$

and  $\theta_{UDC}$  represents the corresponding crank angle when the slider reaches its upper dead center at  $t=0$ .

$\theta(t)$  belongs to  $[\theta_{UDC}, \theta_{UDC} + 2\pi]$  and is a Bezier curve that represents the angular displacement of the input link defined by control points  $\theta_i$ 's. Parameter  $t$  is regarded as the normalized time from 0 to 1. One of the advantages for choosing a Bezier curve for

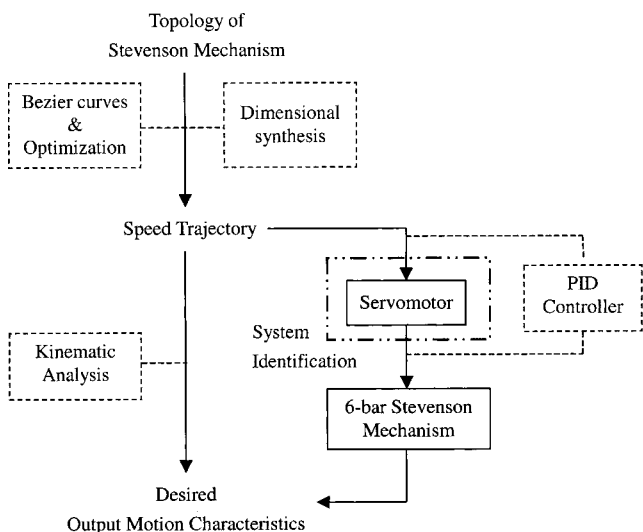


Fig. 1 System flow chart

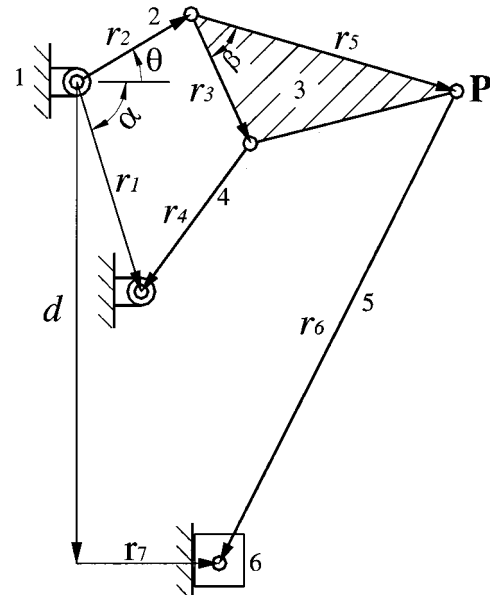


Fig. 2 The Stevenson-type mechanism

motion trajectory is that this curve is  $n$ th order differentiable, which guarantees smoothness of the entire motion. Hence, the angular velocity  $\omega(t)$  and acceleration  $\alpha(t)$  of the input link can be derived by continuously differentiating Eqs. (1)–(2) with respect to time as:

$$\omega(t) = \frac{d\theta(t)}{dt} = \sum_{i=0}^n \theta_i \frac{dB_{i,n}(t)}{dt} \quad (3)$$

$$\alpha(t) = \frac{d^2\theta(t)}{dt^2} = \sum_{i=0}^n \theta_i \frac{d^2B_{i,n}(t)}{dt^2} \quad (4)$$

where  $dB_{i,n}(t)/dt$  and  $d^2B_{i,n}(t)/dt^2$  are derivatives of  $B_{i,n}(t)$  from Eq. (2).

The computation from input motion characteristics, Eqs. (1), (3), and (4), to output motion characteristics is based on vector loop approach (Hall [13]). The ram motion trajectories such as linear displacement, velocity, and acceleration are thus computed, not shown for short, and denoted as  $d(t)$ ,  $v(t)$  and  $a(t)$ .

## 4 Optimization

The derived motion curves on the input link, Eqs. (1), (3), and (4), contain undetermined control points  $\theta_0, \theta_1, \dots, \theta_n$ . Since  $\theta_0$  and  $\theta_n$  are the boundary conditions for crank angles in a cycle,  $\theta_0=0$  and  $\theta_n=2\pi$  must be specified, and  $\theta_{UDC}$  in Eq. (1) makes  $\theta(0)$  and  $\theta(1)$  equal to  $\theta_{UDC}$  and  $\theta_{UDC}+2\pi$ . The remaining control points  $\theta_1, \dots, \theta_{n-1}$  become the design variables that are selected by optimization method.

The optimization is formulated as:

$$\text{Minimize } f_A(\theta_1, \dots, \theta_{n-1}) \quad (5)$$

Subject to

$$\text{equality constraints } h_j(\theta_1, \dots, \theta_{n-1})=0 \quad j=1, \dots, n_h \quad (6)$$

and

$$\text{inequality constraints } g_k(\theta_1, \dots, \theta_{n-1}) < 0 \quad k=1, \dots, n_g \quad (7)$$

where  $n_h$  and  $n_g$  denote the number of equality and inequality constraints. The objective function  $f_A(\theta_1, \dots, \theta_{n-1})$  is to improve the output characteristics of the mechanism. It is usually selected to minimize the peak acceleration, jerk, or a combination of both of the output motion or to reduce the required torque or speed variation of the motor. If the output peak acceleration  $a(t)$  and input speed variation  $\Delta\omega(t)$  are the subjects, the objective function is:

$$f_A(\theta_1, \dots, \theta_{n-1}) = w_1 \cdot \frac{\text{peak}(a(t))}{\text{reference}(a(t))} + w_2 \cdot \frac{\text{peak}(\Delta\omega(t))}{\text{average}(\omega(t))} \quad 0 \leq t \leq 1 \quad (8)$$

where  $w_1$  and  $w_2$  are weighting factors while  $\text{reference}(a(t))$  and  $\text{average}(\omega(t))$  are used for normalizing. The equality and inequality constraints are defined to meet the desired output motion characteristics.

Guidelines for defining the constraints are:

1 Motion continuity for Bezier curves is automatically satisfied at all points except at the boundary where  $t=0$  and  $t=1$ . Hence, continuity at the boundary must be specified manually. Equality constraints can be defined for this purpose as:

$$h_1(\theta_1, \dots, \theta_{n-1}) = \omega(0) - \omega(1) = 0 \quad (9)$$

$$h_2(\theta_1, \dots, \theta_{n-1}) = \alpha(0) - \alpha(1) = 0 \quad (10)$$

2 If at some instants  $t_1$ , the ram must pass through a specified position  $S_1$ , an equality constraint should be defined as:

$$h_3(\theta_1, \dots, \theta_{n-1}) = \theta(t_1) - \theta|_{d=S_1} = 0 \quad (11)$$

3 If constant velocity in a specified period for the output link is required, inequality constraints is defined as:

$$g_1(\theta_1, \dots, \theta_{n-1}) = \int_{t=t_{c1}}^{t=t_{c2}} |v(t) - v(t_{c1})| dt - \varepsilon < 0 \quad (12)$$

where  $\varepsilon$  is a small number. The satisfaction of this constraint forces the output velocity  $v(t)$  during the period from  $t_{c1}$  to  $t_{c2}$  to be approximately a constant.

4 If a quick-return mechanism with specified time ratio  $r$  is the object of the design, an equality constraint is added as:

$$h_4(\theta_1, \dots, \theta_{n-1}) = \theta(t_{return}) - \theta|_{d=Stroke} = 0 \quad (13)$$

where  $t_{return}$  is the time at which the ram reaches its dead point of return, and  $\theta|_{d=Stroke}$  represents its corresponding crank angle.

5 If at some instants  $t_3$  and  $t_4$ , the velocity or acceleration must not exceed a specified value, inequality constraints should be added as:

$$g_2(\theta_1, \dots, \theta_{n-1}) = v(t_3) - v_{lim\ it} < 0 \quad (14)$$

$$g_3(\theta_1, \dots, \theta_{n-1}) = a(t_4) - a_{lim\ it} < 0 \quad (15)$$

Additional constraints should be defined with specific cases and applications.

Now, all information needed for optimization is derived. Any optimization method can be used to determine the design variables  $\theta_1, \theta_2, \dots, \theta_{n-1}$ . Substituting  $\theta_1, \theta_2, \dots, \theta_{n-1}$  into Eq. (3), the desired crank's speed trajectory  $\omega(t)$  becomes:

$$\omega(t) = \sum_{i=0}^n \theta_i \frac{dB_{i,u}(t)}{dt} = \omega(\theta_1, \dots, \theta_{n-1}, t) \quad (16)$$

## 5 Dimensional Synthesis

When designing a new press, proper dimensional synthesis may further reduce the input speed variation of the mechanism. The Stevenson's mechanism, Fig. 2, can be divided into a 4-bar linkage and a mechanism with its slider driven by the coupler point of the 4-bar linkage. Therefore, the motion characteristics of the output link are greatly related to the shape of the coupler curve traced by point **P**. Here, we include dimensional properties as addition design variables and rewrite the optimization problem as:

$$\text{Minimize } f_B(\theta_1, \dots, \theta_{n-1}, r_1, r_2, r_3, r_4, r_5, r_6, r_7, \alpha, \beta) \quad (17)$$

Subject to

equality constraints

$$h_j(\theta_1, \dots, \theta_{n-1}, r_1, r_2, r_3, r_4, r_5, r_6, r_7, \alpha, \beta) = 0 \quad (18)$$

and

inequality constraints

$$g_k(\theta_1, \dots, \theta_{n-1}, r_1, r_2, r_3, r_4, r_5, r_6, r_7, \alpha, \beta) \leq 0 \quad (19)$$

For the mechanism to run continuously, the input link must be a crank. And, the geometric dimensions has to satisfy Grashof criteria [14] as:

$$g_4(\theta_1, \dots, \theta_{n-1}, r_1, r_2, r_3, r_4, r_5, r_6, r_7, \alpha, \beta) = (r_{\max} + r_{\min}) - (r_a + r_b) < 0 \quad (20)$$

$$h_5(\theta_1, \dots, \theta_{n-1}, r_1, r_2, r_3, r_4, r_5, r_6, r_7, \alpha, \beta) = r_2 - r_{\min} = 0 \quad (21)$$

where  $r_{\max}$  and  $r_{\min}$  represent the largest and the smallest link lengths among  $r_1, r_2, r_3, r_4$  while  $r_a$  and  $r_b$  represent the other two link-lengths.

Moreover, it is reasonable for the slider stroke of the resulting mechanism to remain the same as that of the target press. Therefore, another equality is defined as:

$$h_6(\theta_1, \dots, \theta_{n-1}, r_1, r_2, r_3, r_4, r_5, r_6, r_7, \alpha, \beta) = \max(d(t)) - \min(d(t)) = Stroke \quad (22)$$

In this manner, the results will not only the optimal dimensions of the mechanism, but also the useful crank's input speed trajectory.

## 6 Examples

Design examples are provided to demonstrate the procedures for upgrading a regular Stevenson press to a multi-action one. We start from the Bliss press, whose dimensions are  $r_1 = 276.08$ ,  $r_2 = 81.16$ ,  $r_3 = 142.12$ ,  $r_4 = 243.49$ ,  $r_5 = 204.63$ ,  $r_6 = 367.30$ ,  $r_7 = -141.69$ ,  $\beta = 0$  deg,  $\alpha = 90$  deg, running at average crank speed 60 rpm. In what follows, we provide input speed trajectories to perform both deep drawing and precision cutting.

**Example 1: Deep Drawing Process—With Speed Trajectory Planning Only.** The task is to provide the mechanism with a useful output speed trajectory for deep drawing. The input speed trajectory of the crank is the motion to plan. A 10th order Bezier curve, Eqs. (1)–(2) with  $n=10$ , is used to represent the trajectory of the crank displacement.

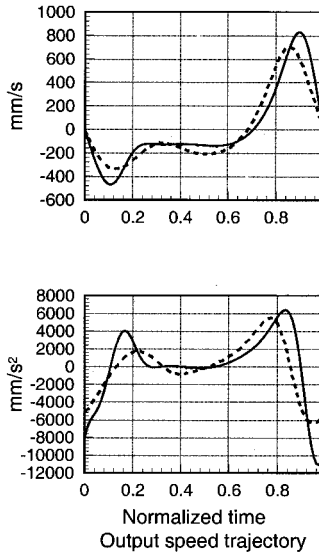
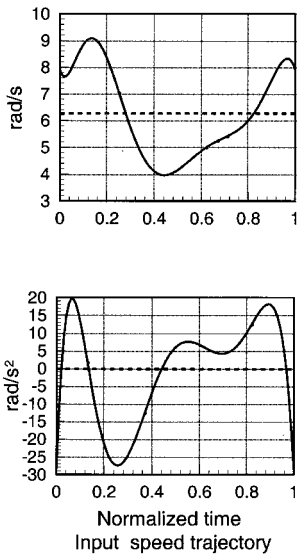
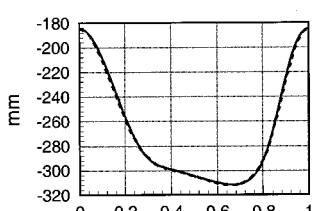
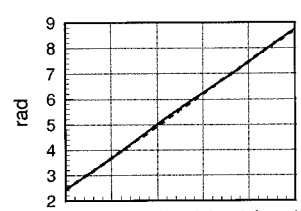
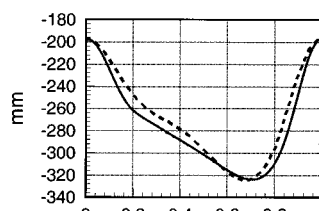
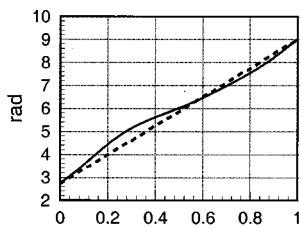


Fig. 3 Speed trajectory planning only—Input and output speed trajectories for deep drawing

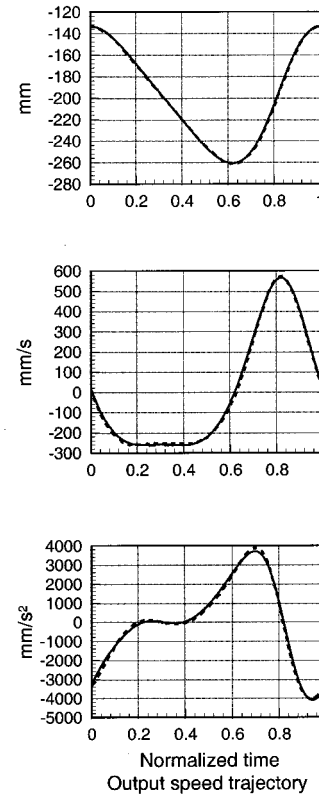
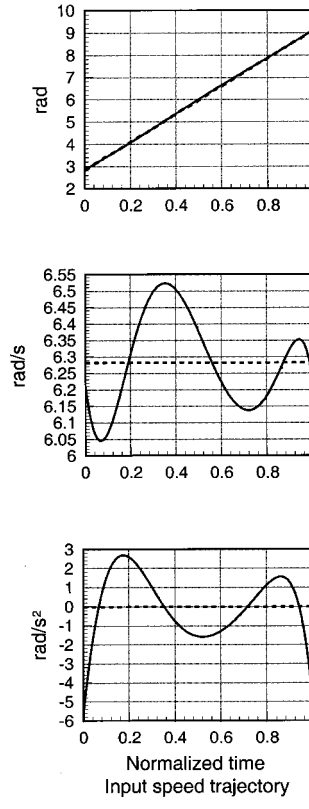


Fig. 4 Combined with dimensional synthesis for deep drawing—Input and output speed trajectories for deep drawing

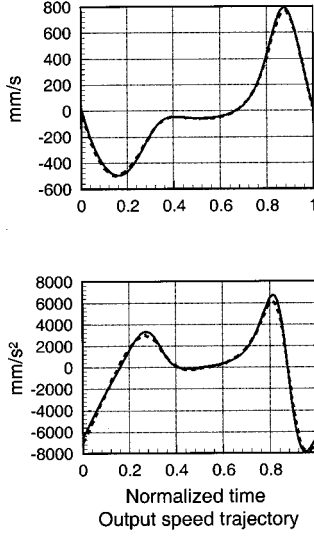
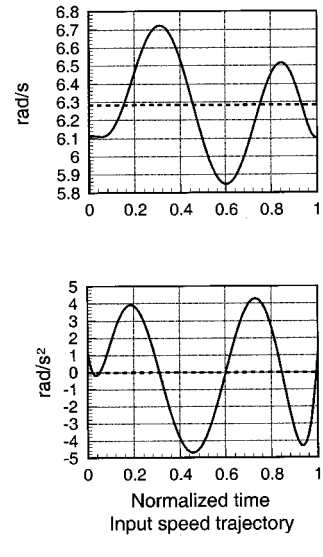


Fig. 5 Combined with dimensional synthesis for precision cutting—Input and output speed trajectories for precision cutting

Recall that  $\theta_0=0$  and  $\theta_n=2\pi$  are the boundary conditions. The remaining control points  $\theta_1, \dots, \theta_9$  are determined through optimization procedure, Eqs. (8)–(10), and the following constraint:

$$g_1(\theta_1, \dots, \theta_9) = \int_{t=0.25}^{t=0.45} |v(t) - v(0.25)| dt - 0.5 < 0 \quad (23)$$

By a recursive quadratic programming subroutine, CVM01, the optimal control points  $\theta_1, \dots, \theta_9$  are obtained as 45.28 deg, 72.20 deg, 227.50 deg, 129.42 deg, 177.28 deg, 205.48 deg, 261.855 deg, 251.08 deg, and 314.72 deg, respectively. The corresponding input and output motion characteristics are shown in Fig. 3. Note that the dotted curves, also in Figs. 4 and 5, show the motion for the same mechanism with constant input for comparison. Therefore, by providing the input angular velocity trajectory, during the working period of the press between  $t=0.25$  and  $0.45$ , the output velocity remain constant for the need of deep drawing.

**Example 2: Deep Drawing and Precision Cutting Processes—With Dimensional Synthesis.** For precision cutting, the ram speed must be slow and remain constant during cutting. The formulation of optimization is the same as in Example 1 except that extra design variables  $r_1, r_2, r_3, r_4, r_5, r_6, r_7, \alpha, \beta$  and extra constraints, Eqs. (11)–(14), (20)–(22), are concerned. The resulting  $r_1, r_2, r_3, r_4, r_5, r_6, r_7, \alpha, \beta$  for deep drawing are 271.07, 51.16, 153.56, 246.25, 301.98, 365.36, -141.72, 0 deg, 86.52 deg, and  $\theta_1, \theta_2, \dots, \theta_9$  are 35.57 deg, 67.63 deg, 104.90 deg, 146.53 deg, 183.39 deg, 217.92 deg, 253.89 deg, 285.32 deg, and 324.42 deg, respectively. As for precision cutting, the resulting  $r_1, r_2, r_3, r_4, r_5, r_6, r_7, \alpha, \beta$  are 262.10, 95.83, 145.13,

234.37, 160.88, 360.26, -131.38, 0 deg, 83.12 deg, and  $\theta_1, \dots, \theta_9$  are 34.96 deg, 70.67 deg, 100.18 deg, 154.33 deg, 196.60 deg, 211.93 deg, 241.58 deg, 290.80 deg, and 325.04 deg, respectively. The corresponding motion characteristics are shown in Figs. 4 and 5. The required ram motion can be achieved when the input link is running at the given speed trajectory. It is noticed that the input speed variation in Fig. 4 is reduced from that in Fig. 3 since the geometric dimensions are also considered in optimization.

## 7 Conclusions

This paper presents a concept of using a servo approach for Stevenson-type presses. The motivation is to come up with a new generation of presses that can be used for various types of press works to upgrade an existing press. It uses a servomotor as the power input. By properly designing the input speed, the output motion can pass through a desired trajectory. The input motion characteristics are planned with Bezier curves containing undetermined control points that are selected by optimization methods to satisfy the design constraints and improve the performance of the system. The guidelines for transferring the design problem into the optimization problem are discussed. Additional dimensional synthesis is also discussed to reduce input speed variation. Examples are given. The success of these examples demonstrates the practicability of this idea of multi-function presses. As long as the servomotor can generate sufficient torque to keep the input speed along the pre-determined speed trajectory, the output motion for multi-action is then achievable.

## Acknowledgment

The authors are grateful to the National Science Council (TAIWAN) for supporting this research under grant NSC88-2212-E-006-013.

## References

- [1] Ulas, I., and Craggs, G., 1995, "Analysis of the Mechanics of Die Drawing Polypropylene Through Strain Rate Controlled Dies," *Proc. R. Soc. London, Ser. A*, **209**, pp. 59-68.
- [2] Tesar, D., and Matthew, G. K., 1976, *The Dynamic Synthesis, Analysis and Design of Modeled Cam Systems*, Lexington Books.
- [3] Yan, H. S., and Fong, M. K., 1994, "An Approach for Reducing the Peak Acceleration of Cam-follower Systems Using a B-spline Representation," *Chinese S. of Mech. Engr. (Taiwan)*, **15**, No. 1, pp. 48-55.
- [4] Yan, H. S., Hsu, M. H., Fong, M. K., and Hsieh, W. H., 1994, "A Kinematic Approach for Eliminating the Discontinuity of Motion Characteristics of Cam-follower Systems," *J. of Applied Mechanisms & Robotics*, **1**, No. 2, pp. 1-6.
- [5] Yan, H. S., Tsai, M. C., and Hsu, M. H., 1996, "A Variable-speed Method for Improving Motion Characteristics of Cam-follower Systems," *ASME J. Mech. Des.*, **118**, No. 1, pp. 250-258.
- [6] Yan, H. S., Tsai, M. C., and Hsu, M. H., 1996, "An Experimental Study of the Effects of CAM speed on Cam-follower systems," *Mech. Mach. Theory*, **31**, No. 4, pp. 397-412.
- [7] Connor, A. M., Douglas, S. S., and Gilmartin, M. J., 1995, "The Synthesis of Hybrid Five-bar Path Generating Mechanisms Using Genetic Algorithms," *IEEE Genetic Algorithms in Engineering Systems: Innovations and Applications*, pp. 213-318.
- [8] Herman, J., Van de Straete, J., and de Schutter, Joris, 1996, "Hybrid Cam Mechanism," *IEEE/ASME Trans. Mechatron.*, **1**, No. 4, pp. 284-289.
- [9] Yossifon, S., Messerly, D., Kropp, E., Shivpuri, R., and Altan, T., 1991, "A Servo Motor Driven Multi-action Press for Sheet Metal Forming," *Int. J. Mach. Tools Manuf.*, **31**, No. 3, pp. 345-359.
- [10] Yossifon, S., and Shivpuri, R., 1993, "Analysis and Comparison of Selected Rotary Linkage Drives for Mechanical Press," *Int. J. Mach. Tools Manuf.*, **33**, No. 2, pp. 175-192.
- [11] Yossifon, S., and Shivpuri, R., 1993, "Optimization of a Double Knuckle Linkage Drive With Constant Mechanical Advantage for Mechanical Presses," *Int. J. Mach. Tools Manuf.*, **33**, No. 2, pp. 193-208.
- [12] Yossifon, S., and Shivpuri, R., 1993, "Design Considerations for the Electric Servomotor Driven 30 Ton Double Knuckle Press for Precision Forming," *Int. J. Mach. Tools Manuf.*, **33**, No. 2, pp. 209-222.
- [13] Hall, A. S., Jr., 1981, *Notes on Mechanism Analysis*, BALT Publishers.
- [14] Hall, A. S., Jr., 1961, *Kinematics and Linkage Design*, BALT Publishers.

## Design of a PZT Bimorph Actuator Using a Metamodel-Based Approach

### David J. Cappelleri

Graduate Research Assistant

### Mary I. Frecker

Assistant Professor

### Timothy W. Simpson

Assistant Professor

Pennsylvania State University, Department of Mechanical and Nuclear Engineering, University Park, PA 16802

### Alan Snyder

Associate Professor, Pennsylvania State University, Department of Surgery, Hershey, PA 17033

*The design of a variable thickness piezoelectric bimorph actuator for application to minimally invasive surgery is proposed. The actuator is discretized into five segments along its length, where the thicknesses of the segments are used as design variables in the problem of optimizing both the force and deflection at the tip. Metamodeling techniques are used to construct computationally inexpensive approximations of finite element simulations and to rapidly explore the design space and the Pareto frontier. A prototype device and experimental verification of the analytical results are also discussed. [DOI: 10.1115/1.1446866]*

**Keywords:** Piezoelectric Bimorph, Minimally Invasive Surgery, Sizing Optimization, Metamodeling

## 1 Introduction

A piezoelectric bimorph actuator consists of a thin passive beam sandwiched between layers of piezoelectric ceramic material (PZT). When opposing voltages are applied to the two ceramic layers, a bending moment is induced in the beam (Fig. 1) [1]. A pair of cantilevered piezoelectric bimorph actuators can be used as a simple grasping device, where the bimorph actuators act as "fingers" (Fig. 2). Similar grasping designs have been developed for MEMS and robotics by Chonan et al. [2] and Seki [3]. Bar-Cohen et al. [4] and Lumia and Shahinpoor [5] have designed bimorph actuator grippers using electroactive polymers.

The focus in this paper is on the design of a PZT bimorph grasper for application to minimally invasive surgical (MIS) procedures. During MIS, small surgical tools and viewing equipment are introduced into a body cavity through several 3-10 millimeter incisions. MIS reduces tissue trauma and patient recovery time compared to open surgery [6,7]; however, there is a need for improved dexterity and control in MIS tools [8-11]. We propose the use of an active end-effector such as a PZT bimorph grasper, where the localized actuation at the working jaws of the end-effector allows for precise control of its position.

The tip deflection and force are critical in such a design, as the jaws of the grasper must deflect to close completely while exert-

Contributed by the Mechanisms & Robotics Committee for publication in the JOURNAL OF MECHANICAL DESIGN. Manuscript received December 1999. Associate Editor: J. S. Rastegar.

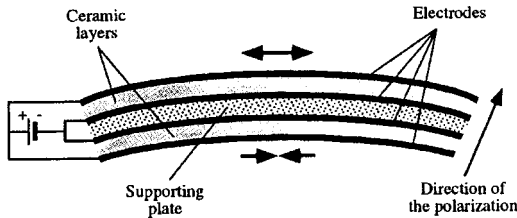


Fig. 1 PZT bimorph

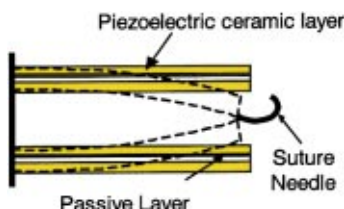


Fig. 2 Bimorph grasper



Fig. 3 Finite element model of variable thickness bimorph actuator

ing a large force to secure tissue or a suture needle. The deflection and force are determined by the geometry of the actuator, the material properties, and the applied voltage. Since the operating frequency is low (on the order of 1–2 Hz) in MIS applications, only quasi-static response is considered. Using simple models of a standard bimorph actuator with constant layer thicknesses, the blocked force available at the tip (force exerted with no deflection), and the free tip deflection were calculated. It was determined that a standard bimorph of appropriate size for MIS provides insufficient grasping force and tip deflection [12]. To improve the deflection and force performance of the bimorph actuator, a variable thickness design is proposed where the thickness of the piezoceramic layers is varied along the length. The finite element model for the bimorph actuator is described next.

## 2 Finite Element Model

Finite element analysis of the bimorph actuator is performed using ABAQUS [13] to predict the free tip deflection and the blocked force while subjecting the actuator to a prescribed input voltage. The actuator is modeled as composite beam with a thin steel passive layer sandwiched between layers of PZT5H [14]. The bimorph actuator is 54.0 mm long and 3.0 mm wide. The PZT layers are discretized into five sections, where the thickness of the sections,  $t_i$  ( $i = 1, \dots, 5$ ), are the design variables. Posing the problem in terms of discrete section thicknesses rather than a continuously varying shape limits solutions to those that are easily fabricated from commercially available PZT ceramic material. The finite element model consists of 1944 eight-node three-dimensional (brick) elements with cantilever supports at the root nodes (Fig. 3). Each PZT section has three elements across its height and width and 10 elements along the length. As the thickness of the PZT sections is varied in the optimization procedure, the number of elements remains constant.

In the FEA simulations, each PZT section is driven at its saturation voltage so that the maximum induced strain in each PZT

section can be obtained. The saturation voltage is the maximum allowable voltage and is proportional to the thickness of the PZT material. By operating each segment at its saturation voltage, the voltage is varied along the length of the bimorph actuator, resulting in dramatic improvements in the tip deflection and force compared to the same bimorph operated at a constant voltage.

## 3 Solution Approach

A metamodel-based approach is employed in this study to simultaneously maximize tip deflection and blocked force of the bimorph actuator. Metamodelling involves the use of design of experiments [15] and metamodels (e.g., response surfaces [16]) to sample a design space and construct inexpensive-to-run approximations of a computationally expensive computer analysis like ABAQUS. The approximations are then used in lieu of ABAQUS to rapidly explore the design space during optimization; a detailed explanation of our approach is given in [17].

For this study, a half-fraction central composite face-centered (CCF) design [16] is used to sample each design variable at one of three levels: 1.0 mm, 2.0 mm, and 3.0 mm. The CCF design allows us to sample the free deflection and blocked force of the PZT bimorph actuator at 27 points in ABAQUS to generate enough data to build approximations for tip deflection and blocked force. Two different types of metamodels—response surface models and kriging models—are employed to construct approximations from this sample data. The response surface models used in this study are second-order polynomial models of the form:

$$\hat{y}(t) = \beta_0 + \sum_{i=1}^5 \beta_i t_i + \sum_{i=1}^5 \beta_{ii}^2 t_i^2 + \sum_{i=1}^5 \sum_{j=1}^5 \beta_{ij} t_i t_j \quad (1)$$

where  $\hat{y}(t)$  is the predicted response,  $t_i$  are the design variables, and  $\beta_{ij}$  are the coefficients used to fit the model. A complete description of response surface modeling can be found in, e.g., [16]. Note that although the metamodels are constructed using a set of points at three discrete levels, the optimization solutions found using the metamodels need not be restricted to these discrete values.

Since response surface models are typically second-order polynomial models, they have limited capability to accurately model non-linear functions of arbitrary shape. Therefore, as part of this study we are investigating kriging models as alternatives to response surface models. Kriging models are interpolative approximations based on an exponentially weighted sum of the sample data [18,19]. The kriging models used in this study consist of constant underlying “global” models combined with Gaussian correlation functions based on the results of our previous studies [20,21]. To ensure that both sets of approximations are sufficiently accurate for use during optimization, the metamodels are validated using 25 additional points from ABAQUS [12].

## 4 Optimization Results

One advantage of using approximations such as response surface and kriging models is that the design space can be rapidly explored to examine the tradeoff between competing design objectives. For this example, a  $5^5$  search grid (3125 points) is used to explore the design space and predict the Pareto frontier. The Pareto frontier can be thought of as a “trade-off curve” of design points in the performance space, beyond which it is not possible to improve both objectives. A formal procedure for efficiently estimating the Pareto frontier using metamodels is presented in [17]. As seen in Fig. 4, the Pareto frontier can be readily captured using the metamodels themselves without using any optimization or a weighted-sum of the objectives with varying weights. The kriging model is a better predictor of force and deflection, while the response surface models are poor predictors of designs with large deflections.

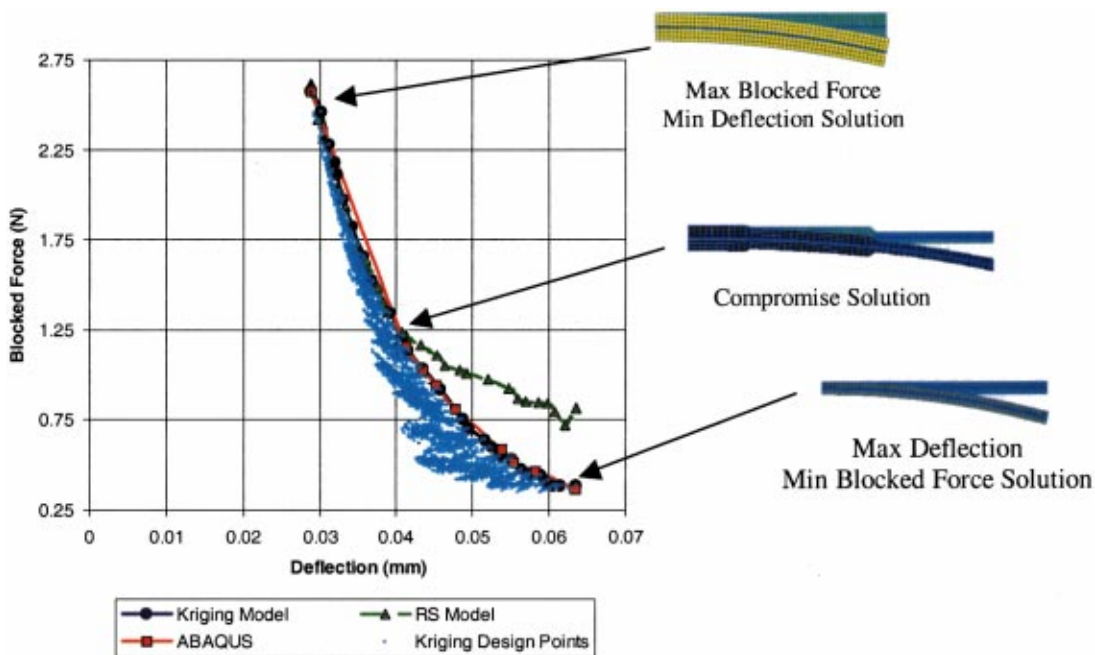


Fig. 4 Design space and Pareto frontier

It is evident from Fig. 4 that the Pareto frontier is not concave, indicating that a unique maximum combination of force and deflection does not exist. The maximum force solution is a thick bimorph actuator, where all the design variables are at their upper limits, while the maximum deflection solution is thin, where all the design variables are at their lower limits. A tapered design is selected as a compromise solution with section thicknesses of 2.5 mm, 2.0 mm, 2.0 mm, 1.0 mm, and 1.0 mm. This solution pro-

vides sufficient force performance for the intended MIS application. The kriging models predict  $F_{blocked} = 1.21$  N and  $\delta_{free} = 0.0411$  mm, which compare well with values obtained from ABAQUS (1.16 N and 0.0413 mm, respectively).

## 5 Experimental Results

A scaled prototype of the compromise design was constructed and tested in the laboratory. The free deflection was measured using a laser vibrometer, and the blocked force was measured using a 500 g load cell. The experimental setup is pictured in Fig. 5, and the data is shown in Fig. 6. The ABAQUS model under-predicts the free deflection and over-predicts the blocked force significantly at high voltage levels. This difference between the experimental data and the FEA predictions is attributed to the presence of the epoxy bonding layer, which is not accounted for in the finite element model.

## 6 Closing Remarks

A variable thickness PZT bimorph actuator design is proposed, where the PZT material is discretized into five segments along the length. It is desired to maximize both the tip deflection and blocked force of the actuator for application to minimally invasive surgical procedures. A metamodel-based approach is employed in this work to rapidly explore the design space and identify candidate designs along the Pareto frontier. The kriging models predict tip deflection and blocked force more accurately, particularly for the designs with high deflection and low blocked force. The plot of the Pareto frontier reveals that a unique maximum does not exist for this problem, but a compromise design is selected that provides sufficient force. A prototype of the compromise design was constructed, and experimental testing reveals that the bonding layer may significantly affect the performance of the bimorph actuator.

## Acknowledgments

The support of the Charles E. Culpeper Foundation Biomedical Pilot Initiative is gratefully acknowledged by the first two authors. Support from ONR Contract # N00039-97-D-0042 is also acknowledged by the third author.

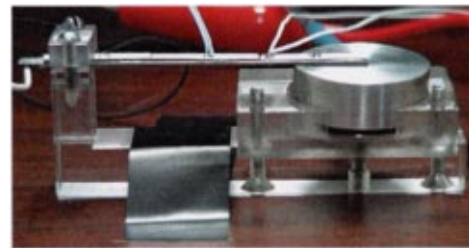


Fig. 5 Experimental setup

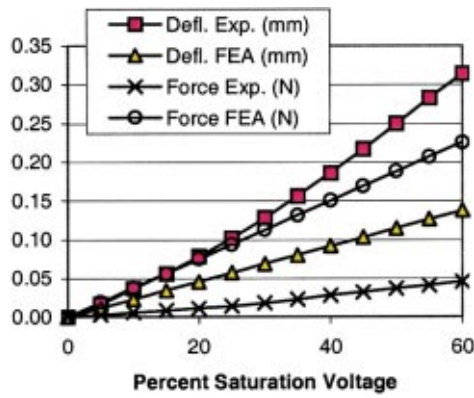


Fig. 6 Experimental data and FEA prediction

## References

[1] Fatikow, S., and Rembold, U., 1997, *Microsystem Technology and Microrobotics*, Springer-Verlag Berlin Heidelberg.

[2] Chonan, S., Jiang, Z. W., and Koseki, M., 1996, "Soft-handling Gripper Driven by Piezoceramic Bimorph Strips," *Smart Mater. Struct.* **5**, pp. 407-414.

[3] Seki, H., 1992, Piezoelectric Bimorph Microgripper Capable of Force Sensing and Compliance Adjustment. *Japan/USA Symposium on Flexible Automation*, ASME 1992, **1**, pp. 707-713.

[4] Bar-Cohen, Y., Leary, S., Shahinpoor, M., Harrison, J. O., and Smith, J., 1999, "Flexible Low-Mass Devices and Mechanisms Actuated by Electro-Active Polymers," *Proceedings SPIE Smart Structures and Materials*, **3669**, pp. 51-56.

[5] Lumia, R., and Shahinpoor, M., 1999, Microgripper Using Electro-Active Polymers. *Proceedings SPIE Smart Structures and Materials* **3669**, pp. 322-329.

[6] Soper, N. J., Brunt, L. M., and Kerbl, K., 1994, Laparoscopic General Surgery, *N. Engl. J. Med.* Feb. 10, 1994, **330**, No. 6, pp. 409-419.

[7] Soper, N. J., Odem, R. R., Clayman, R. V., and McDougall, E. M., (editors) 1994, *Essentials of Laparoscopy*, Quality Medical Publishing, Inc., St. Louis.

[8] Cohn, M., Crawford, L., Wendlandt, J., and Sastry, S., 1995, "Surgical Applications of Milli-Robots," *J. Rob. Syst.*, **12**, No. 6, pp. 401-416.

[9] Hill, J., and Jensen, J., 1998, "Telepresence Technology in Medicine: Principles and Applications," *Proc. IEEE* **86**, No. 3, March, 1998, pp. 569-580.

[10] Melzer, A., 1996, *Endoscopic Instruments—Conventional and Intelligent, Endosurgery*, Churchill Livingstone, New York, pp. 69-95.

[11] Sastry, S., Cohn, M., and Tendick, F., 1997, "Millirobotics for Remote Minimally Invasive Surgery," *Rob. and Auto. Syst.* **21**, pp. 305-316.

[12] Cappelleri, D. J., Frecker, M. I., and Simpson, T. W., 1999, "Optimal Design of a PZT Bimorph Actuator for Minimally Invasive Surgery," *7th International Symposium on Smart Structures and Materials*, Newport Beach, CA, SPIE, March 5-9, 1999.

[13] ABAQUS Version 5.7-1, 1997, Hibbit, Karlsson and Sorensen, Inc., 1080 Main Street, Pawtucket, Rhode Island 02860.

[14] IEEE Group on Sonics and Ultrasonics, Transducers and Resonators Committee, *IEEE Standard on Piezoelectricity (176-1978)*, ANSI/IEEE, New York, 1978.

[15] Montgomery, D. C., 1997, *Design and Analysis of Experiments*, Fourth Edition, John Wiley & Sons, New York.

[16] Myers, R. H., and Montgomery, D. C., 1995, *Response Surface Methodology: Process and Product Optimization Using Designed Experiments*, John Wiley & Sons, New York.

[17] Wilson, B., Cappelleri, D. J., Frecker, M. I., and Simpson, T. W., 2001, "Efficient Pareto Frontier Exploration Using Surrogate Approximations," *Opt. Eng.*, **2**, 31-50.

[18] Sacks, J., Welch, W. J., Mitchell, T. J., and Wynn, H. P., 1989, Design and Analysis of Computer Experiments. *Stat. Sci.* **4**, No. 4, pp. 409-435.

[19] Koehler, J. R., and Owen, A. B., 1996, "Computer Experiments," *Handbook of Statistics (Ghosh, S. and Rao, C. R., eds.)*, Elsevier Science, New York, pp. 261-308.

[20] Simpson, T. W., Mauery, T. M., Korte, J. J., and Mistree, F., 1998, "Comparison of Response Surface and Kriging Models for Multidisciplinary Design Optimization," *7th AIAA/USAF/NASA/ISSMO Symposium on Multidisciplinary Analysis & Optimization*, St. Louis, MO, AIAA, **1**, pp. 381-391. AIAA-98-4755.

[21] Jin, R., Chen, W., and Simpson, T. W., 2000, September 6-8, "Comparative Studies of Metamodelling Techniques under Multiple Modeling Criteria," *8th AIAA/NASA/USAF/ISSMO Symposium on Multidisciplinary Analysis and Optimization*, Long Beach, CA, AIAA, AIAA-2000-4801.